AGU PUBLICATIONS

Water Resources Research

RESEARCH ARTICLE
10.1002/2017WR021061

Implementing Dynamic Root Optimization in Noah-MP for Simulating Phreatophytic Root Water Uptake

Ping Wang[1,2,3], Guo-Yue Niu[2,3], Yuan-Hao Fang[2,3,4], Run-Jian Wu[2,3], Jing-Jie Yu[1,5], Guo-Fu Yuan[6], Sergey P. Pozdniakov[7], and Russell L. Scott[8]

[1]Key Laboratory of Water Cycle and Related Land Surface Processes, Institute of Geographic Sciences and Natural Resources Research, Chinese Academy of Sciences, Beijing, China, [2]Department of Hydrology & Atmospheric Sciences, University of Arizona, Tucson, AZ, USA, [3]Biosphere 2, University of Arizona, Oracle, AZ, USA, [4]Department of Hydrology and Water Resources, Hohai University, Nanjing, China, [5]College of Resources and Environment, University of Chinese Academy of Sciences, Beijing, China, [6]Key Laboratory of Ecosystem Network Observation and Modeling, Institute of Geographic Sciences and Natural Resources Research, Chinese Academy of Sciences, Beijing, China, [7]Department of Hydrogeology, Moscow State University, Moscow, Russia, [8]Southwest Watershed Research Center, USDA-ARS, Tucson, AZ, USA

Key Points:
- Root acts as a flexible regulator in the plant's functioning and surviving
- A soil moisture-dependent root dynamics scheme (VOM-ROOT) was implemented in Noah-MP
- The coupled model reproduces the observed root profile and improves the transpiration simulation under a hyperarid climate

Correspondence to:
P. Wang,
wangping@igsnrr.ac.cn;
G.-Y. Niu,
niug@email.arizona.edu

Citation:
Wang, P., Niu, G.-Y., Fang, Y.-H., Wu, R.-J., Yu, J.-J., Yuan, G.-F., et al. (2018). Implementing dynamic root optimization in Noah-MP for simulating phreatophytic root water uptake. *Water Resources Research*, *54*, 1560–1575. https://doi.org/10.1002/2017WR021061

Received 5 MAY 2017
Accepted 15 FEB 2018
Accepted article online 20 FEB 2018
Published online 5 MAR 2018

Abstract Widely distributed in arid and semiarid regions, phreatophytic roots extend into the saturated zone and extract water directly from groundwater. In this paper, we implemented a vegetation optimality model of root dynamics (VOM-ROOT) in the Noah land surface model with multiparameterization options (Noah-MP LSM) to model the extraction of groundwater through phreatophytic roots at a riparian site with a hyperarid climate (with precipitation of 35 mm/yr) in northwestern China. VOM-ROOT numerically describes the natural optimization of the root profile in response to changes in subsurface water conditions. The coupled Noah-MP/VOM-ROOT model substantially improves the simulation of surface energy and water fluxes, particularly during the growing season, compared to the prescribed static root profile in the default Noah-MP. In the coupled model, more roots are required to grow into the saturated zone to meet transpiration demand when the groundwater level declines over the growing season. The modeling results indicate that at the study site, the modeled annual transpiration is 472 mm, accounting for 92.3% of the total evapotranspiration. Direct root water uptake from the capillary fringe and groundwater, which is supplied by lateral groundwater flow, accounts for approximately 84% of the total transpiration. This study demonstrates the importance of implementing a dynamic root scheme in a land surface model for adequately simulating phreatophytic root water uptake and the associated latent heat flux.

1. Introduction

A phreatophyte, which means "well plant" in Greek, is a deep-rooted plant that has the ability to obtain a perennial supply of water from the phreatic zone (or saturated zone) and/or the capillary fringe above the phreatic zone in the soil profile (Meinzer, 1927). Extensive reports indicated that phreatophytic vegetation is widely distributed in the arid and semiarid regions of southern Canada (Meyboom, 1965), the southwestern United States (Cleverly et al., 2006; Cooper et al., 2006; Devitt et al., 2011; Steinwand et al., 2006; Stromberg et al., 2007), western Australia (Eamus et al., 2006; Sommer & Froend, 2011), southern Africa (Le Maitre et al., 1999), and northwestern China (Gries et al., 2003; Wang et al., 2014a; Yuan et al., 2014).

Plant roots act as a key mediator for transpiration (Warren et al., 2015) and play a critical role in acquiring water and nutrients from the soil (Orellana et al., 2012). Phreatophytes in arid regions are mostly dependent on groundwater: their roots penetrate the unsaturated zone, extend to the capillary fringe and the saturated zone (Gary, 1963; Naumburg et al., 2005; Stromberg et al., 2007) and extract moisture directly from groundwater (Ehleringer & Dawson, 1992; Le Maitre et al., 1999; Scott et al., 2004). This has been evidenced by diurnal fluctuations in the groundwater level (e.g., Gribovszki et al., 2010; Loheide et al., 2005; Miller et al., 2010; Wang et al., 2014b; Wang & Pozdniakov, 2014; White, 1932) and soil moisture above the water table (Nachabe et al., 2005). Recent reports indicate that phreatophytes in arid climates are not water stressed because they directly access groundwater through their roots (Glenn et al., 2013); as a result, a substantial amount of root water uptake may come from groundwater, especially for gradual water table declines (Lowry & Loheide, 2010).

Another important feature of phreatophytes is a survival strategy that involves self-optimizing root systems, which evolve to access groundwater while coping with potentially anaerobic or saline groundwater conditions (Canham et al., 2012; Fan et al., 2017; Orellana et al., 2012). In response to declines in the water table, rapid root growth (up to 15 mm/d) toward the water table has been observed for desert phreatophytes (Naumburg et al., 2005; Orellana et al., 2012; Vonlanthen et al., 2010), including *Populus*, *Salix*, and *Tamarix* species (Fenner et al., 1984; Horton & Clark, 2001; Kranjcec et al., 1998). In a hyperarid climate, the vigor of phreatophytes in riparian zones has been shown to be highly dependent on their rooting depth relative to the water table depth and the associated capillary fringe (Eamus et al., 2015; Stromberg, 2013).

The root dynamics of phreatophytes in response to fluctuations in the groundwater level are well recognized (Canham et al., 2012; Tron et al., 2015). However, most current land surface models (LSMs) and terrestrial biosphere models used in Earth system models (ESMs) (e.g., Niu et al., 2011; Oleson et al., 2010; Warren et al., 2015) do not represent root dynamics; instead, they prescribe a static root profile for all plant types through two type-dependent parameters: maximum rooting depth and vertical root distribution (Jackson et al., 2000). In many models, the root profile during a simulation is fixed as a uniform, exponential, or asymptotic profile (Hao et al., 2005; Smithwick et al., 2014). This relatively simple treatment of plant roots may result in significant biases when simulating surface water, energy, and carbon flux exchanges with the atmosphere, especially in dry climates.

Warren et al. (2015) highlighted the need to enhance root functionality in large-scale, process-based LSMs by introducing dynamic root distributions and root functional traits. For example, Gayler et al. (2014) implemented a root-growth scheme in the Noah-MP LSM to account for the impact of unfavorable temperature and soil moisture conditions on deep roots. A recent review (Smithwick et al., 2014) suggested that LSMs should adequately represent the adaptation and evolution of root systems to account for direct access to deep soil water and thus improve the modeling of ecosystem response to seasonal droughts. Numerous modeling studies have followed a general approach based on the evolutionary optimization concept, which was introduced into plant ecophysiology in the 1970s (e.g., Cowan, 1978; Orians & Solbrig, 1977; Westoby, 1979). Some models assume that plant roots have the ability to respond dynamically to changes in climate, soil, and vegetation characteristics, resulting in different rooting depths depending on the water-use strategy (intensive or conservative) of different plants (Guswa, 2008, 2010). Other modeling approaches provide insight into the adaptation of the root profile to varying precipitation, soil moisture, and groundwater (Gou & Miller, 2014) to maximize plant carbon gain (Kleidon & Heimann, 1998) and transpiration (Rudd et al., 2014). Similarly, the Vegetation Optimality Model (VOM) developed by Schymanski et al. (2009) assumes that vegetation properties can be optimally adapted to environmental conditions (Schymanski et al., 2015) and that the root profile can be optimized to minimize plant water stress (Schymanski et al., 2008) while maximizing carbon gain (Schymanski et al., 2009). Schymanski et al. (2008) showed that the VOM improved the simulation of soil moisture and respiration at a tropical savanna site and resulted in a more realistic root response to the transition between wet and dry seasons.

There are two general approaches to modeling root water uptake: microscopic (or mesoscopic) models describe the water absorption of single roots, whereas macroscopic models describe the root density distribution, which proportionally controls root water uptake from different soil layers (Šimůnek & Hopmans, 2009). In this paper, we followed the macroscopic approach and implemented the root dynamics of VOM into the Noah-MP LSM (Niu et al., 2011). We aim to quantify the extraction of groundwater through phreatophytic roots at a riparian site in a hyperarid climate (with precipitation of 35 mm/yr) in northwestern China. The original VOM was a coupled ecohydrological model of vegetation dynamics and subsurface hydrology (Schymanski et al., 2008). In this study, we only coupled the root dynamics component of VOM (hereafter, VOM-ROOT) with the hydrology in Noah-MP. We tested the coupled Noah-MP/VOM-ROOT model against in situ measurements of soil moisture and surface energy and water fluxes and then quantified the root water uptake fluxes from different layers of the unsaturated and saturated zones.

2. Model Description

2.1. Noah-MP

Noah-MP numerically describes the energy, water, and carbon flux exchanges between the land surface and the atmosphere that are controlled by terrestrial ecohydrological processes (Ma et al., 2017; Niu et al.,

2011). Based on Noah (Chen & Dudhia, 2001; Ek et al., 2003), Noah-MP was first augmented with vegetation and groundwater dynamics (Niu et al., 2007) and provides multiple schemes for various processes, with each scheme representing a different interpretation (or hypothesis) of the same individual process.

Noah-MP solves the one-dimensional (1-D) Richards equation to compute vertical soil moisture distribution using the Clapp-Hornberger retention relationship (Clapp & Hornberger, 1978). The upper boundary condition for soil moisture is the infiltration rate, which is computed as the residual of precipitation minus surface runoff and parameterized through a simple TOPMODEL-based runoff scheme (Niu et al., 2005). Noah-MP treats unconfined aquifers as a reservoir or "bucket" underlying the soil column to account for water exchanges between the vadose zone and the aquifer through gravity and capillary forces (Niu et al., 2007).

Noah-MP explicitly represents evaporation from the soil surface (E_{dir}, m s^{-1}), canopy interception loss (E_c, m s^{-1}), and transpiration (E_t, m s^{-1}) through formulations analogous to Ohm's law, considering the aerodynamic and stomatal resistance to water vapor flux within and over plant canopies. Plant transpiration is limited by stomatal resistance. Stomatal resistance is linked to photosynthesis, which is controlled by a soil moisture availability factor (or β factor) and the maximum carboxylation rate under optimum conditions, V_{cmax} (a vegetation type-dependent constant). Noah-MP uses a static root profile scheme in which the roots are assumed to be evenly distributed in the vertical direction because of a lack of predictive understanding of the interactions between water and root dynamics.

Noah-MP represents plant photosynthesis and respiration following the dynamic vegetation model of Dickinson et al. (1998). However, the schemes for carbon assimilation through photosynthesis of sunlit and shaded leaves involve parameterizations of radiation transfer and multiple scattering of light by leaves and the ground, limitations of Rubisco, light, transport of photosynthate, and PEP-carboxylase (Collatz et al., 1992, 1991; Farquhar et al., 1980), as well as numerous uncertain parameters. Additionally, the respiration and allocation of assimilated carbon into various plant parts (wood, stem, leaves, and roots) are determined empirically and highly parameterized (e.g., Dickinson et al., 1998; Gim et al., 2017; Lacointe, 2000). The primary motivation for this study is to examine root optimization in response to water table dynamics but not carbon dynamics: parameterizations associated with the coupled root and carbon dynamics model are not included.

2.2. VOM-ROOT Dynamics

VOM-ROOT assumes that plants have an evolving mechanism that can minimize the "costs" of maintaining their root system while meeting their water demands. VOM-ROOT operates in three steps. First, it predicts plant water storage, i.e., the total amount of liquid water stored in living tissues per unit ground area, M_q (kg m^{-2}) (Figure 1), as follows:

$$\frac{\partial M_q}{\partial t} = \rho_w \left(\sum_{i=1}^{N_r} Q_{r,i}(t) - E_t(t) \right), \tag{1}$$

where ρ_w is the density of water (1,000 kg m^{-3}), $Q_{r,i}$ is the rate of water uptake by roots in soil layer i (m s^{-1}), N_r is the number of soil layers that contain roots, and E_t is the transpiration rate (m s^{-1}). $Q_{r,i}$ is assumed to withdraw water from the ith soil layer in proportion to the pressure gradient between the root suction head ($h_{r,i}$, m) and the matric suction head (h_i, m) (Figure 1). By analogy to Ohm's law,

$$Q_{r,i} = S_{Ar,i} J_{r,i} = S_{Ar,i} \left(\frac{h_{r,i} - h_i}{\Omega_r + \Omega_{s,i}} \right), \tag{2}$$

where $S_{Ar,i}$ is the root area index (RAI), which is defined as the root surface area per unit ground area in layer i (m^2 m^{-2}), $J_{r,i}$ is the water uptake per unit RAI in layer i (m s^{-1}), Ω_r is the root radial resistance to water flow through the roots per unit RAI, and $\Omega_{s,i}$ is the resistance to water flow through soil particles toward the root surface in the ith layer (s). $h_{r,i}$ is determined by the tissue balance pressure in aboveground plant organs, which provides a driving force for passive water uptake by roots. More details on $h_{r,i}$ and $\Omega_{s,i}$ can be found in Schymanski et al. (2008).

Second, VOM-ROOT determines whether the actual root surface area is adequate to withdraw sufficient water to meet a plant's water demands for transpiration over the previous day. This can be numerically described through the plant water storage capacity M_{qx} (kg m^{-2}), i.e., the maximum plant water storage. If

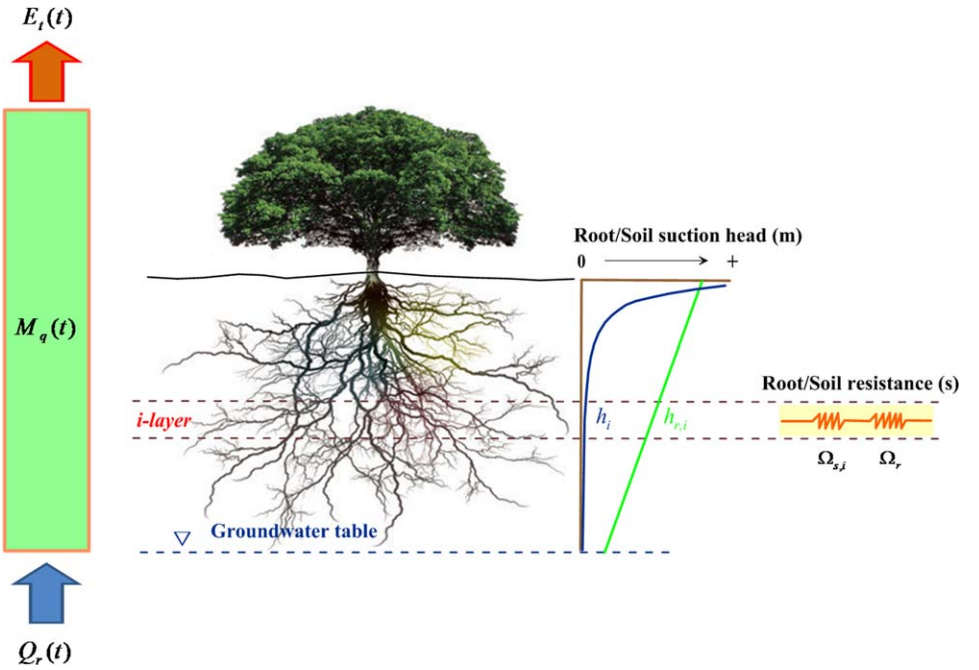

Figure 1. Schematic diagram of the VOM-ROOT model. (left) For the water stored in living plant tissues, including the below-ground and above-ground biomass, E_t represents the transpiration rate, Q_r represents the total root water uptake, and M_q represents the water stored in plant tissues per unit ground area. (right) For the root water uptake processes, Ω_r represents the resistance to water flow through the roots per unit root surface area, $\Omega_{s,i}$ represents the resistance to water flow toward the root surface through the *i*th layer soil particles, and h_i and $h_{r,i}$ represent the matric suction head and root suction head, respectively, of layer *i*.

the actual plant water storage (M_q) predicted by equation (1) always exceeds 95% of M_{qx}, the root surface area is more than adequate and the root surface area will decrease. In contrast, if M_q falls below 95% of M_{qx}, the root surface area will increase. Once M_q falls below a critical threshold, $M_{q\min}$ (kg m^{-2}), which is assumed to be 0.9 M_{qx} by Schymanski (2007), the root surface area cannot meet the demand for transpiration, leading to stomatal closure to prevent further depletion of M_q. Therefore, a coefficient of change for the root system (k_r) is defined as follows:

$$k_r = \frac{0.95M_{qx} - M_q}{0.05M_{qx}}, \tag{3}$$

where M_q ranges between $0.9M_{qx}$ and M_{qx}. Thus, the value of k_r varies between 1 and -1, indicating an increase (when $M_q \leq 0.95M_{qx}$) or a reduction in roots (when $M_q > 0.95M_{qx}$), respectively.

The last step is to determine where the roots grow depending on the water uptake rate of a layer during the previous day. A relative growth rate ($k_{\text{reff},i}$) for each layer of roots is defined as the ratio of the water uptake rate of a root layer during the previous day ($J_{\text{rdaily},i}$) to the water uptake rate by the most effective root layer during that previous day, as follows:

$$k_{\text{reff},i} = \frac{0.5J_{\text{rdaily},i}}{\max\left(J_{\text{rdaily},i}\right)} \tag{4}$$

The daily change in root surface area density (i.e., the daily change in root surface area per unit soil volume in each soil layer, $\Delta S_{Adr,i}$) is then updated as a function of k_r and $k_{\text{reff},i}$, as follows:

$$\Delta S_{Adr,i} = G_{\text{rmax}}\, k_{\text{reff},i} k_r, \tag{5}$$

where G_{rmax} is the maximum daily root-growth rate (m^2 m^{-3}), which depends on vegetation type. k_r determines when the roots grow, and $k_{\text{reff},i}$ determines where the roots grow. When $k_r > 0$, the root surface area grows more rapidly in wetter soil layers with a larger value of $k_{\text{reff},i}$ in response to a larger $J_{\text{rdaily},i}$ according to equation (4). However, when $k_r < 0$, the root surface area shrinks more rapidly in wetter layers in the

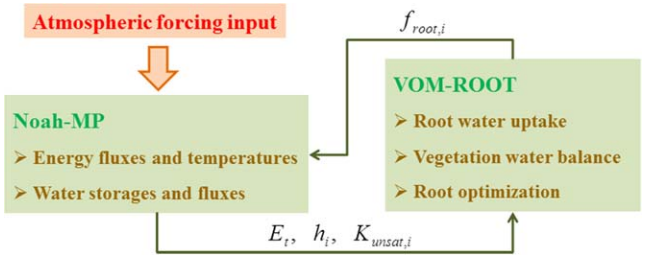

Figure 2. Schematic diagram showing the coupling between VOM-ROOT and Noah-MP. E_t is the transpiration rate; h_i and $K_{unsat,i}$ are the matric suction head and unsaturated hydraulic conductivity, respectively, in soil layer *i*; and $f_{root,i}$ is the vertical root fraction in the *i*th layer.

same manner as represented in equation (4). As a net result, equation (4) cannot produce a root profile with more roots in wetter soil layers. For this reason, we modified $k_{reff,i}$ in equation (4) for $k_r < 0$ to $k_{reff,i} = \max\left(J_{rdaily,i}\right)/J_{rdaily,i}$ to reduce the rate of root surface area shrinking in wetter soil layers.

2.3. Coupling VOM-ROOT and Noah-MP

We coupled VOM-ROOT with Noah-MP by exchanging state and flux variables between the two models. Noah-MP provides VOM-ROOT with transpiration (E_t), matric suction head (h_i), and hydraulic conductivity ($K_{unsat,i}$); VOM-ROOT, in turn, transfers its vertical root distribution to Noah-MP (Figure 2).

In Noah-MP, the plant transpiration E_t is linearly related to the soil moisture controlling factor (β) through modification of the stomatal resistance. $\beta = \sum_1^{N_r} \beta_i$, where β_i is the soil moisture controlling factor of *i*th soil layer. β_i is determined by the root fraction ($f_{root,i}$, dimensionless) and the soil moisture in liquid form ($\theta_{liq,i}$, $m^3\ m^{-3}$) in the *i*th layer, as follows:

$$\beta_i = f_{root,i} \min\left(1.0,\ \frac{\theta_{liq,i} - \theta_{wilt}}{\theta_{ref} - \theta_{wilt}}\right), \tag{6}$$

where θ_{wilt} and θ_{ref} are the soil moisture at the wilting point ($m^3\ m^{-3}$) and a reference soil moisture ($m^3\ m^{-3}$; close to field capacity), respectively. Niu et al. (2011) provide more details for calculating the *ET* flux. Note that the above equation does not represent the adverse effects of anoxic conditions when the soil moisture approaches saturation (Feddes et al., 1978; Šimůnek & Hopmans, 2009). We suggest that equation (6) is appropriate in this study because phreatophytic roots feature aerenchyma, facilitating their adaptation to the anoxic conditions in the saturated zone, although careful consideration may be necessary for other vegetation types.

The representations of h_i and $K_{unsat,i}$ for unsaturated soils follow Clapp and Hornberger (1978):

$$\begin{aligned} h_i &= h_{sat}\left(\theta_i/\theta_{sat}\right)^{-b} \\ K_{unsat,i} &= K_{sat}\left(\theta_i/\theta_{sat}\right)^{2b+3} \end{aligned}, \tag{7}$$

where θ_i is the volumetric soil moisture content (*SMC*) ($m^3\ m^{-3}$) in the *i*th soil layer, θ_{sat} is the saturated water content ($m^3\ m^{-3}$), h_{sat} is the saturated soil water potential (m), K_{sat} is the saturated hydraulic conductivity ($m\ s^{-1}$), and the exponent *b* is an empirical parameter that is dependent on soil texture.

VOM-ROOT provides Noah-MP with the vertical root fraction, which is an average of the dynamic root surface area density ($S_{Adr,i}$) weighted by the layer thickness, Δz_i (m), as follows:

$$f_{root,i} = \frac{\Delta z_i \times S_{Adr,i}}{\sum_{i=1}^{N_r} \left(\Delta z_i \times S_{Adr,i}\right)} \tag{8}$$

In the default model, Noah-MP assumes that the root surface area density is homogeneous, and thus $f_{root,i}$ is only controlled by the layer thickness. Note that the above optimized root fraction through $S_{Adr,i}$ is applicable to both the unsaturated and the saturated zones.

3. Experimental Data

3.1. Experimental Site

The experimental data used in this study were obtained from a *Tamarix* spp. stand (87°54′E, 40°27′N, with an altitude of 846 m) in the lower Tarim River Basin (Yuan et al., 2014). The Tarim River is the longest and largest inland river in northwestern China, flowing through deserts and recharging riparian areas via ephemeral riverbed infiltration. The study area is characterized by a hyperarid climate with annual precipitation of only 34 mm (Yuan et al., 2014), potential evaporation of approximately 1340 mm/yr (according to

Table 1
Soil Physical Properties Based on Laboratory Analyses

	Soil physical properties					Soil texture
Depth (m)	Sand (2–0.05 mm) (%)	Silt (0.05–0.002 mm) (%)	Clay (<0.002 mm) (%)	Bulk density (g cm^{-3})	Saturated hydraulic conductivity (m s^{-1})	USDA classification
0.1	No data	No data	No data	1.10	2.74×10^{-5}	
0.3	80	17	3	No data	No data	Loamy sand
0.4	No data	No data	No data	No data	2.35×10^{-5}	
0.6	17	72	11	No data	No data	Silt loam
1.0	15	77	8	No data	No data	Silt loam
1.5	34	59	7	1.41	1.70×10^{-6}	Silt loam
2.0	48	47	5	No data	No data	Sandy loam
2.5	43	52	5	No data	No data	Silt loam
3.0	37	57	6	No data	No data	Silt loam
4.0	22	69	9	No data	No data	Silt loam
5.0	44	51	5	No data	No data	Silt loam

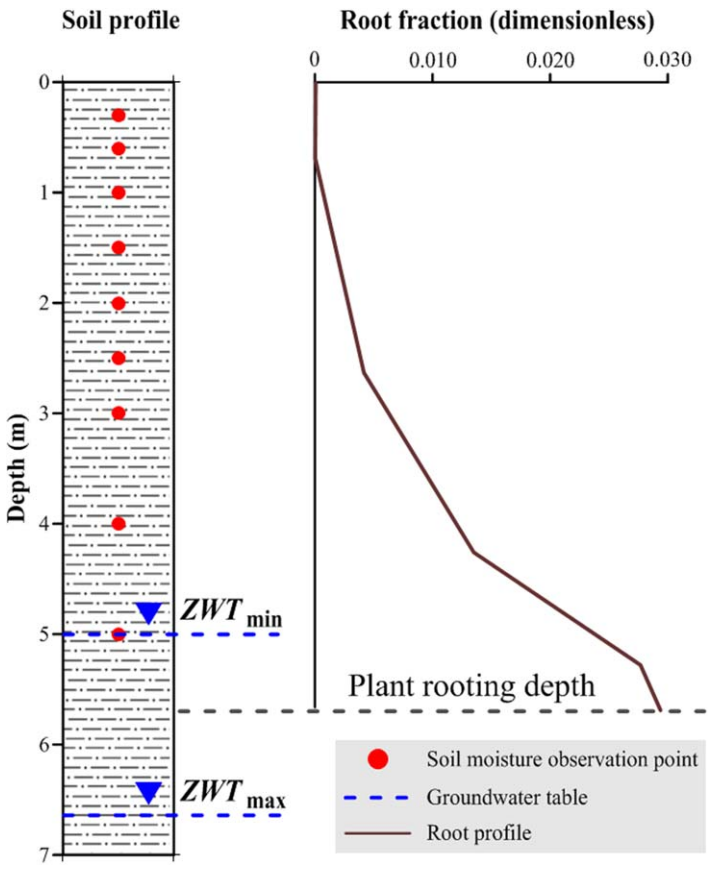

Figure 3. Diagram showing (left) the locations of the soil moisture sensors and groundwater levels and (right; see Xu et al., 2011, for details) the root fraction in each 5 cm soil layer measured at a nearby site with similar hydroclimate and vegetation conditions. ZWT_{min} and ZWT_{max} represent the minimum and maximum depths of the water table, respectively (see also the observed water table depth in Figure 5).

the nearby Tikanlik meteorological station) (Han & Hu, 2012), and an annual mean temperature of 11°C (Yuan et al., 2014).

The dominant vegetation types along the river are phreatophytes (e.g., *Populus euphratica* and *Tamarix* spp.), which rely heavily on groundwater from shallow alluvial aquifers that are recharged by the river during flood periods (Ye et al., 2009). The approximately 200 m × 300 m of riparian shrubland selected includes *Tamarix ramosissima*, *Tamarix hispida*, and *Tamarix elongate* along with a small amount of herbaceous plants under the shrubs. The total vegetation cover fraction was 0.65, and the leaf area index (*LAI*) was 1.15 m^2 m^{-2} during the early growing season of 2012 (Yuan et al., 2014). The top 5 m of the soil profile is a silt loam mixed with a loamy sand, and K_{sat} decreases with depth (ranging from 2.74×10^{-5} to 1.70×10^{-6} m s^{-1}; Table 1).

3.2. Measurements

The energy fluxes between the land surface and the atmosphere, including both latent heat (*LE*, W m^{-2}) and sensible heat (*H*, W m^{-2}), were measured using the eddy-covariance (EC) system described by Yuan et al. (2014). Soil heat flux plates were installed 8 cm below the soil surface, and the ground heat flux (*G*, W m^{-2}) was calculated based on an estimate of the change in heat storage in the soil above the plates. Meteorological variables, including air temperature, air pressure, wind speed, relative humidity, and rainfall, were measured on site. In addition, nine frequency domain capacity (FDC) sensors (FDS100, Unism, Beijing, China) were installed at soil depths of 0.3, 0.6, 1.0, 1.5, 2.0, 2.5, 3.0, 4.0, and 5.0 m to measure the soil volumetric water content (Figure 3). Furthermore, a 20 m deep well located 30 m from the flux tower was set up to monitor groundwater level changes. All measurements were recorded at 30 min intervals. Root profile measurements from a nearby site with similar hydroclimate and vegetation conditions (Figure 3) (Xu et al., 2011) were used for a comparison to the modeled root fraction.

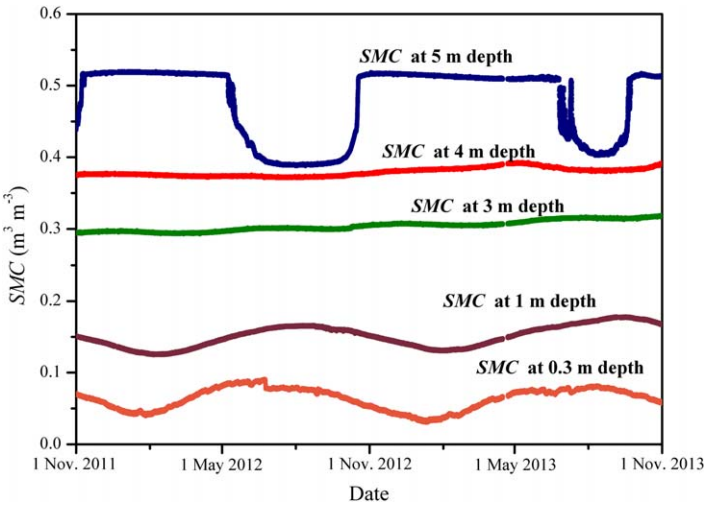

Figure 4. Observed 30 min liquid soil moisture content (*SMC*, $m^3\ m^{-3}$) at 0.3, 1, 3, 4, and 5 m depths.

We collected more than 2 years of data from 8 June 2011 to 8 November 2013; some missing data occurred because of unfavorable meteorological conditions or instrument failures. The model requires continuous meteorological data as its upper boundary condition; therefore, we filled shorter data gaps (less than 1 day) using data recorded at the same time on the previous day. For longer gaps (more than 1 day), we used data recorded on the same day of the previous or the subsequent year. Imbalances in measured surface energy fluxes are often problematic (Heusinkveld et al., 2004; Wilson et al., 2002). In this study, we used an approach similar to that of Twine et al. (2000) to distribute the energy residual between sensible and latent heat fluxes based on the proportion of the daily averaged ratio of sensible to latent heat fluxes (Foken, 2008).

3.3. Evidence of Plant-Groundwater Interactions

Yuan et al. (2014) observed a distinct diurnal fluctuation in the water table during the growing season, indicating direct root water uptake from groundwater. The soil moisture measured at 5 m varied seasonally, from approximately 0.52 $m^3\ m^{-3}$ during the nongrowing season to 0.40 $m^3\ m^{-3}$ during the growing season (Figure 4). However, the soil moisture measured at shallower depths of 4 and 3 m remained stable at approximately 0.38 $m^3\ m^{-3}$ and 0.30 $m^3\ m^{-3}$, respectively (Figure 4). These observations suggest that *Tamarix* took up deep soil water and groundwater through its roots. As a result, the water table gradually declined from the beginning (late April) to the middle (early August) of the growing season (Figure 5) but with an increasing trend that was caused by lateral groundwater flow (Wang et al., 2014a, 2014b). It is worth noting that the liquid soil moisture in the upper layers (0–1 m depth) exhibited slight seasonal variations (Figure 4), which are likely associated with seasonal freeze-thaw cycles.

4. Model Experiments

4.1. Soil and Vegetation Parameters

4.1.1. Soil Hydraulic Properties

During the nongrowing season, despite a slight depletion in liquid soil moisture caused by freezing of the upper layer, the soil moisture content in the unsaturated zone remained relatively constant (Figure 4), suggesting a quasi-equilibrium state. Assuming homogeneous soil, we estimated the Clapp-Hornberger parameters (Clapp & Hornberger, 1978) for use in Noah-MP (Table 2) by fitting the retention relationship between the suction head and soil moisture observed during the nongrowing season (Figure 6). As discussed in section 3.3, root water uptake primarily occurs in the deeper soil layers; therefore, we used the observed soil moisture between 3 and 5 m when fitting the relationship.

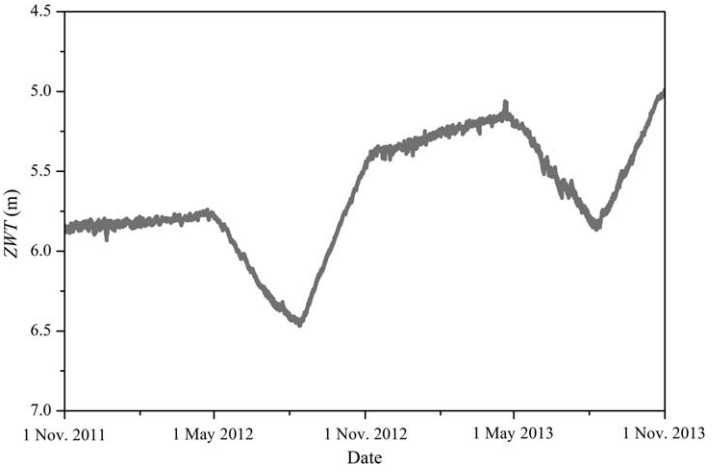

Figure 5. Observed water table depth (*ZWT*) at 30 min intervals.

The soil moisture at the wilting point, θ_{wilt}, was estimated to be 0.048 $m^3\ m^{-3}$ (Table 2), which is equivalent to −3 MPa and is consistent with the estimates provided by Zeng et al. (2002) and Nippert et al. (2010) for the typical riparian shrub *T. ramosissima*. We used Rosetta SSC (with pedotransfer functions of the % sand, silt, and clay) (Schaap et al., 2001) to calculate the saturated hydraulic conductivity, K_{sat}. The resulting K_{sat} value ranged from 4.68×10^{-6} to 7.68×10^{-6} m s^{-1}, with an average value of 6.06×10^{-6} m s^{-1}, which is close to the default value for sandy loam soils in the look-up table of Noah-MP (5.23×10^{-6} m s^{-1}). We used the default values of θ_{ref} and K_{sat} for sandy loam provided by the Noah-MP look-up table (Table 2).

4.1.2. Vegetation Parameters

The vegetation parameters used in VOM-ROOT were modified to approximate *Tamarix* spp. in a dry environment. Based on the data reported in the literature (Gou & Miller, 2014; Vogel et al., 2016; Xu et al., 2011), the mean radius of the fine roots (r_r) was set to 1.0 ×

Table 2
Model Parameters Used in the Simulations

Parameters	Description	Values
Vegetation Parameters[a]		
r_r (m)	Mean radius of fine roots	1.0×10^{-3}
Ω_r (s)	Root radial resistance to water uptake per unit root surface area	8.64×10^{8}
M_d (kg m^{-2})	Mass of dry matter in living plant tissues per unit ground area	5.2
M_{qx} (kg m^{-2})	Water storage capacity of living plant tissues per unit ground area	5.2
c_1 (bar)	Empirical constant used to quantify tissue balance pressure see equation (23) in Schymanski et al. (2008)	750
c_2 (bar)	Empirical constant used to quantify tissue balance pressure see equation (23) in Schymanski et al. (2008)	1
c_{Pbm} (m bar^{-1})	Conversion coefficient from pressure (bar) to hydraulic head (m)	10.2
ρ_w (kg m^{-3})	Density of water	1.0×10^{3}
G_{rmax} (m^2 m^{-3} d^{-1})	Maximum daily root-growth rate	0.1
V_{cmax} (μmol CO$_2$ m^{-2} s^{-1})	Maximum rate of carboxylation	90
LAI (m^2 m^{-2})	Leaf area index	May: 1.0 Jun: 1.8 Jul: 2.6 Aug: 2.6 Sept: 1.5 Oct: 0.4
Soil Hydraulic Properties		
θ_{sat} (m^3 m^{-3})	Saturated water content	0.540
θ_{wilt} (m^3 m^{-3})	Soil moisture at the wilting point	0.048
θ_{ref} (m^3 m^{-3})	Reference soil moisture	0.383
h_{sat} (m)	Saturated soil water potential	0.60
b (dimensionless)	Clapp-Hornberger empirical parameter	2.56
K_{sat} (m s^{-1})	Saturated hydraulic conductivity	5.23×10^{-6}
Model Layers		
Number of layers in the unsaturated zone (−)		100
Layer thickness of the unsaturated zone (cm)		5
Number of layers in the saturated zone (−)		1
Layer thickness of the saturated zone (cm)		65 for DYN-CON 70 for DYN-VAR
Model Spin-Up Time		
Total number of spin-ups (−)		5

[a]The values for the vegetation parameters are from Schymanski et al. (2008), except for r_r, Ω_r, M_d, M_{qx}, V_{cmax}, and *LAI*.

10^{-3} m, and the root resistance to water uptake per unit root surface area (Ω_r) was assumed to be 10,000 days (i.e., 8.64×10^8 s). Anwar and Yin (1997) estimated the mass of dry matter in living plant tissues per unit ground area (M_d) for *Tamarix* spp. in northwestern China to be approximately 5.2 kg m^{-2}. According to Schymanski et al. (2008), the plant water storage capacity (M_{qx}) in VOM-ROOT was assumed to be equal to the mass of dry matter in living plant tissues per unit ground area (M_d). The other plant parameters associated with the root water uptake in equations (1) and (2) and root optimization in equation (5) were the same as those in Schymanski et al. (2008) (see Table 2).

V_{cmax} (μmol CO$_2$ m^{-2} s^{-1}) and *LAI* (m^2 m^{-2}) are key vegetation parameters in Noah-MP that control transpiration and surface energy fluxes. Zhang (2015) performed a parameter sensitivity analysis and concluded that simulated transpiration is generally not very sensitive to estimates with an error of 10–20% in V_{cmax}. Analysis of the current literature data on *Tamarix* spp. collected in northwestern China (Wang et al., 2012) and the Mediterranean basin (Jaoudé et al., 2012; Kuzminsky et al., 2014) suggests that the V_{cmax} value is approximately 90 μmol CO$_2$ m^{-2} s^{-1} (Table 2).

The simulation of *LAI* in Noah-MP involves complex schemes of carbon assimilation via photosynthesis, allocation of carbon to leaves, leaf growth, and maintenance respirations, death attributable to water and temperature stresses, and the resulting feedback to photosynthesis. Although transpiration is primarily controlled by stomatal conductance through light availability and temperature stress, to reduce the effect of errors resulting from uncertain *LAI* simulation on the dynamics of root water uptake, we used *LAI*

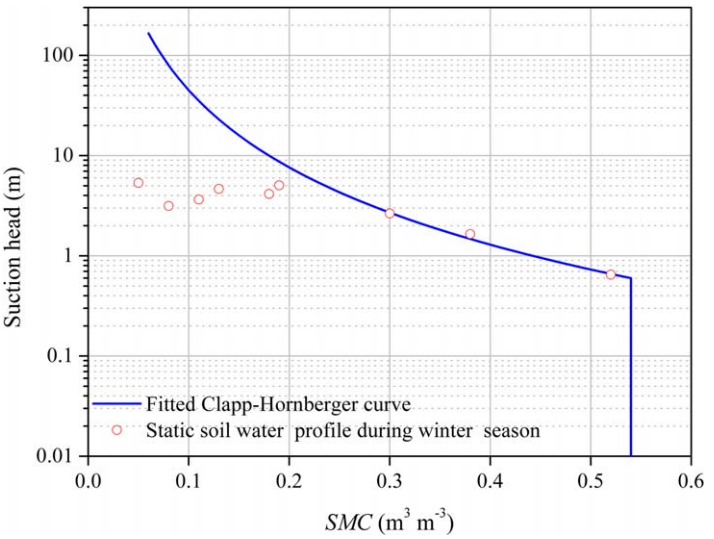

Figure 6. Fitted soil water retention curve using the mean soil moisture content for a static water table depth of 5.65 m during the nongrowing season (between December and March).

measurements to modify the monthly *LAI* look-up table in Noah-MP. At this site, in the early growing season of 2012, *LAI* was 1.15 m^2 m^{-2} (Yuan et al., 2014), and the mean *LAI* during the entire growing season was estimated to be approximately 1.6 m^2 m^{-2} (Zhang, 2015). Because more detailed measurements of seasonal variations in *LAI* were not available, we modified the monthly *LAI* values ranging from 0.4 to 2.6 m^2 m^{-2} (Table 2); these values are consistent with other studies conducted on *Tamarix* spp., which showed a high *LAI* of *Tamarix* spp. (e.g., Glenn & Nagler, 2005; Hultine et al., 2010; Nagler et al., 2004, 2008; Sala et al., 1996) and its seasonal variations (Tian et al., 2004).

4.2. Modeling of the Experimental Site

4.2.1. Model Setup

The model allows the roots to reside in the entire model soil column, including both the unsaturated and the saturated zones; they are evenly distributed at the beginning of the model experiments. Considering that the capillary fringe (i.e., the saturated zone where the matric potential changes but the water content does not (Jury & Horton, 2004)) was 0.60 m thick (Table 2), we assumed that the unsaturated zone was approximately 5.0 m thick. The upper 5.0 m unsaturated zone was then divided into 100 layers, each with a layer thickness of 5 cm; the layer below 5.0 m, including the capillary fringe and saturated zone, was assigned as a single model layer (i.e., the 101st layer). The root surface area density in the entire soil column, including the 101st layer (i.e., the density of waterlogged or phreatophytic roots), was optimized through the dynamic root scheme. The total rooting depth and the layer thickness of the 101st layer (depending on the total rooting depth) was calibrated against the observed ET flux.

4.2.2. Model Experiments

We conducted two experiments with the coupled Noah-MP/VOM-ROOT model. The first experiment (hereafter referred to as "DYN-CON") used a static water table depth of 5.65 m, which is the averaged water table depth during the observation period (Figure 5) without seasonal variations, and the second experiment ("DYN-VAR") used the observed dynamic water table depth varying from 5.0 to 6.5 m (Figure 5). For a fair comparison with DYN-CON, we also conducted a baseline experiment using the default Noah-MP, with an evenly distributed, static root profile across the entire soil column with a rooting depth that is the same as the calibrated rooting depth of DYN-CON.

We used observed near-surface meteorological data, which were available from 8 June 2011 to 8 November 2013, to drive the model. To have three full years for use in the model spin-up runs, we filled the missing data from 1 January 2011 to 7 June 2011 and from 9 November 2013 to 31 December 2013, with data recorded during the same period in adjacent years. To obtain the initial conditions of soil moisture and temperature along with other prognostic variables, we spun the model up for five loops using the 3 year data from 1 January 2011 to 31 December 2013. This 15 year model run also ensured an equilibrium state between the soil moisture and the root dynamics. We used the modeling results from 1 November 2011 to 31 October 2013, from the final loop for analyses.

4.3. Modeling Results

4.3.1. Model Improvements

The baseline experiments using the default Noah-MP with the evenly distributed, static root profile produced reasonable estimates of ground heat (G) and net radiation (R_n) fluxes but poorly partitioned the available energy ($R_n - G$) into latent and sensible heat fluxes. Generally, the model underestimated latent heat flux during the growing season and overestimated the sensible heat flux during the same period to balance the available energy. This feature is partly attributable to the model's failure to reproduce direct root water uptake from the saturated zone, which is considered as a dominant process controlling *ET* of the phreatophytes.

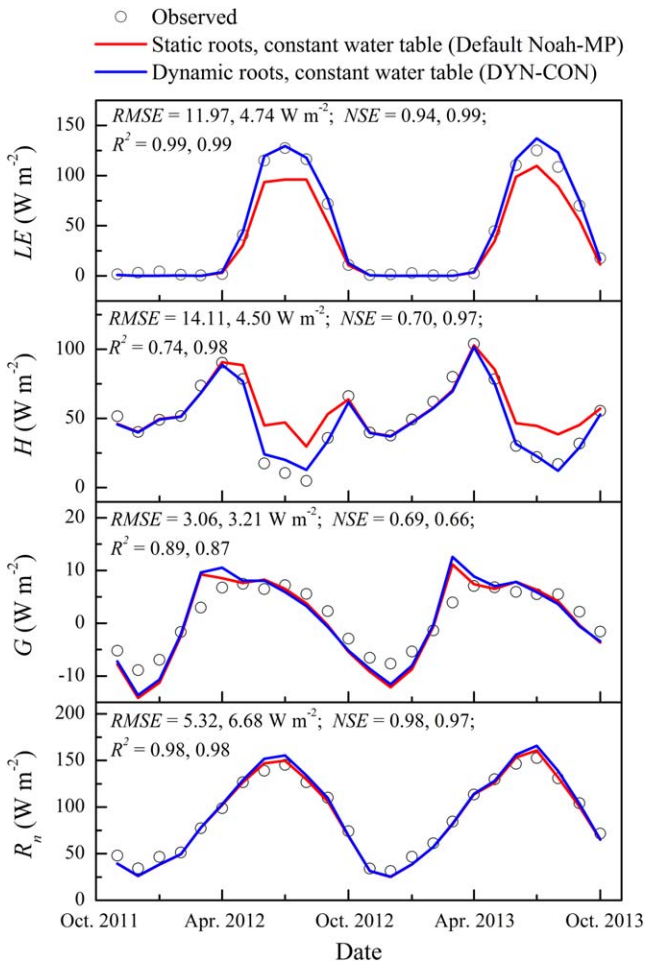

Figure 7. Modeled versus observed monthly latent heat flux (*LE*), sensible heat flux (*H*), ground heat flux (*G*), and net radiation (R_n). Values of the root-mean-square errors (*RMSE*s), Nash-Sutcliffe efficiency (*NSE*), and coefficient of determination (R^2) are presented in the order of default Noah-MP and DYN-CON.

To produce *ET* values that are comparable to the observations (Figure 7), the rooting depth was calibrated to be 5.65 m for DYN-CON, and the resulting root fraction below 5.0 m (i.e., the 101st layer) averaged over the two growing seasons is 0.27. In contrast, for DYN-VAR, the rooting depth was calibrated to be 5.70 m, and the resulting root fraction below 5.0 m increases to 0.44. These results suggest that the declining groundwater levels during the growing seasons (as simulated by DYN-VAR) necessitates the growth of additional roots in the saturated zone to maintain the observed transpiration rates. The calibrated rooting depth (5.70 m) is roughly equal to the average water table depth (5.65 m).

Compared to DYN-CON, the default Noah-MP model with a static root profile was unable to produce accurate simulations of the latent and sensible heat fluxes, as indicated by the root-mean-square errors (*RMSE*s), the Nash-Sutcliffe efficiency (*NSE*), and the coefficient of determination (R^2) (Figure 7). The default Noah-MP underestimated latent heat flux during the growing season even if the total soil depth and the rooting depth were extended from the standard 2.0 m (used in weather forecast and short-term climate prediction models) to 5.65 m, as set in the DYN-CON.

4.3.2. Interactions Between the Soil Moisture Profile and Root Distribution

In the coupled Noah-MP/VOM-ROOT model, the soil moisture and the root profile are tightly coupled. As shown in Figures 8a and 8b, the vertical root distribution above the saturated zone strongly responded to the soil moisture profile, in turn affecting the vertical soil moisture distribution. The modeled and observed soil moisture profiles averaged over the two growing seasons were roughly consistent, but deviate at depths between 2 and 4 m (Figure 8a). These differences are likely related to the model's assumption of evenly distributed soil texture.

In addition, the modeled root fraction profile averaged over the two growing seasons resembles the observed profile at a nearby site with similar hydroclimate and vegetation conditions (Figure 8b) despite the lack of key processes associated with carbon allocation to roots and root turnover in the model. To improve the prediction of soil moisture and root distribution, soil texture data varying among different soil horizons should be included, which would allow the determination of depth-specific hydraulic parameters for the model (Gao et al., 2015).

At this site, the annual *ET* (approximately 515 mm) is much higher than the annual precipitation (approximately 35 mm). The excess of *ET* over precipitation is primarily supplied by direct root water uptake from deep soil moisture and groundwater, which are periodically replenished by infiltrating river water. To satisfy the root water uptake needed for plant transpiration, the modeled root surface area density optimized by VOM-ROOT exhibited significant seasonal variations (Figure 8c).

4.3.3. ET Partitioning and Plant Water-Use Strategies

DYN-VAR reproduced the daily *ET* dynamics (Figure 9a) with high R^2 (0.93) and *NSE* (0.92) values, and a low *RMSE* value (0.50 mm d^{-1}) (Figure 9b). The modeled transpiration (E_t) was 944 mm for the 2 year period, accounting for 92.3% of the total *ET*, whereas the simulated canopy interception loss (E_c) and soil surface evaporation (E_{dir}) were 5 mm (0.5% of the total *ET*) and 74 mm (7.2% of the total *ET*), respectively. The sum of E_c and E_{dir} is roughly equal to the total precipitation (*P*) observed during the same period. In general, canopy interception loss and soil surface evaporation occurred immediately after rainfall events and lasted for a few days (Figure 9c). The low soil evaporation rates in the model are also supported by observations such as the lack of diurnal and seasonal variations in the soil moisture of shallow soils and the presence of a dry surface sandy layer (Yuan et al., 2014). Therefore, in this hyperarid area with root-accessible water tables, plant transpiration is primarily enabled and sustained by optimally adapted deep and vigorous root systems that follow the variations in the water table.

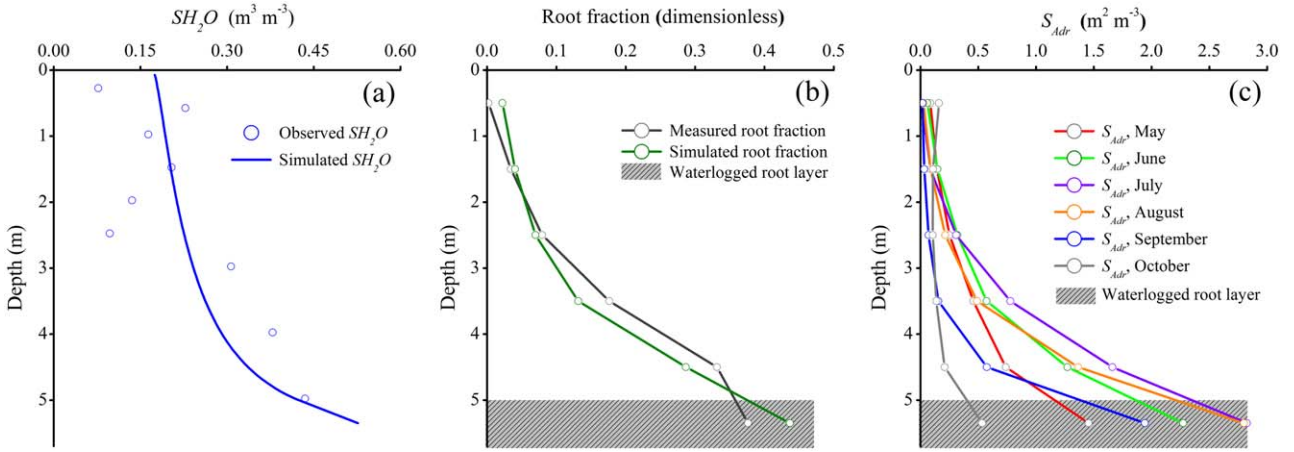

Figure 8. (a) Comparison between the modeled soil moisture profile (liquid water only, SH_2O) and observations. (b) Comparison between the modeled (DYN-VAR) root fraction and observations (Xu et al., 2011) in the upper 5 m unsaturated zone for each 1 m soil layer and in the lower waterlogged root layer (0.7 m) averaged over the two growing seasons. (c) The modeled (DYN-VAR) monthly root surface area density (S_{Adr}) averaged over the two years along the soil depth with intervals, as indicated in Figure 8b.

The coupled Noah-MP/VOM-ROOT modeling results indicate that nearly 84% of the root water uptake for plant transpiration came from shallow groundwater and the capillary fringe above the water table. The lack of seasonal variation in the observed soil moisture in the upper 4 m of the profile (Figure 4) also suggests that active roots are mainly concentrated in the soil layers close to the water table. These results are similar

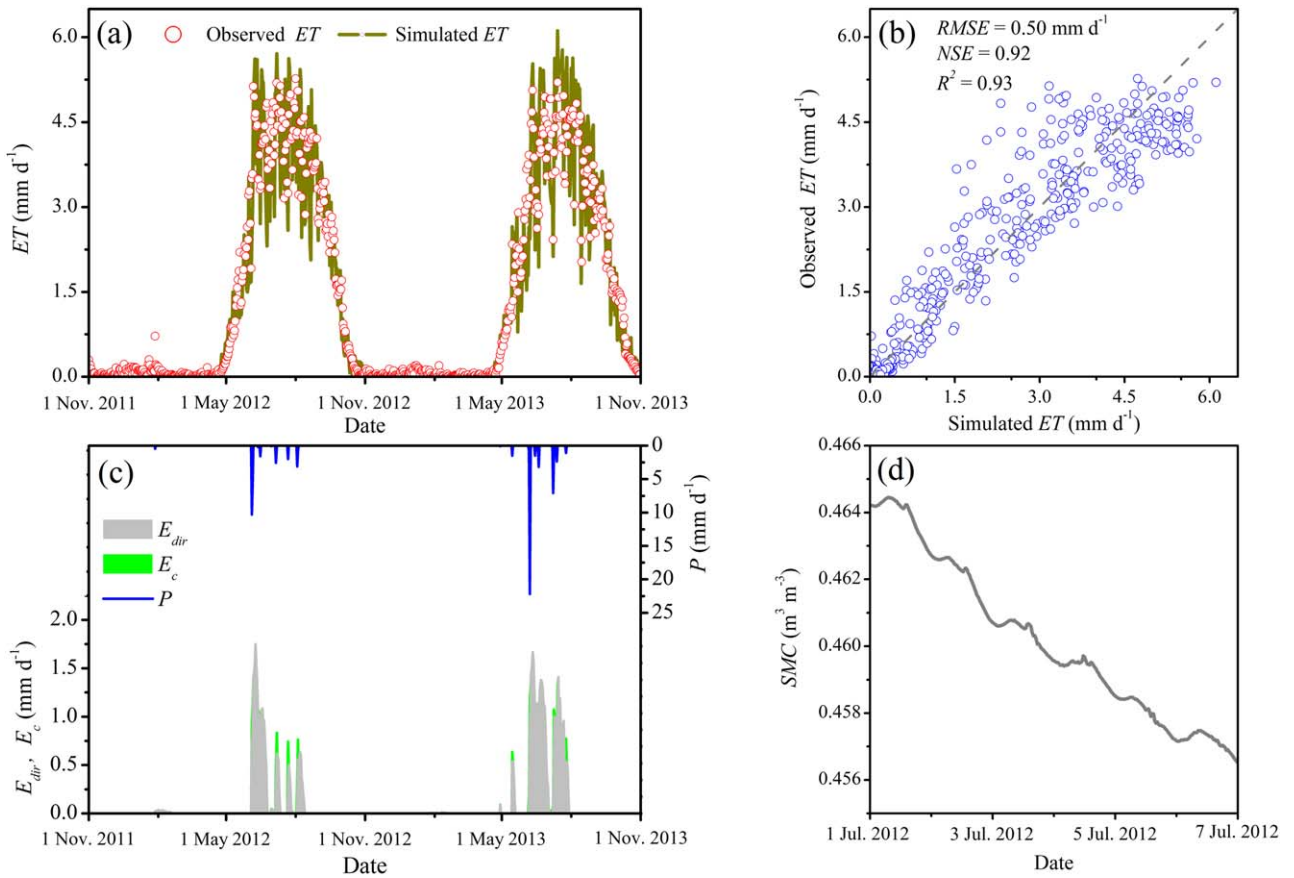

Figure 9. (a) Daily *ET* modeled by DYN-VAR and its observations. (b) Comparison between simulated and observed *ET*. (c) Superimposed canopy evaporation (E_c in green) upon soil evaporation (E_{dir} in light gray) in relation to rainfall events (P in blue). (d) Typical diurnal variations in soil moisture content (*SMC*, in m^3 m^{-3}) in the waterlogged root layer during the growing season.

to the simulations of phreatophytic vegetation in California presented by Gou and Miller (2014), indicating that from 62% to 96% of plant transpiration during the dry season is accounted for by root uptake from groundwater. This modeling result is also consistent with other studies on the water-use strategy of phreatophytic vegetation (Engel et al., 2005; Orellana et al., 2012; Scott et al., 2008).

The modeled diurnal cycle in soil moisture close to the water table during the peak growing season (Figure 9d) is a combined result of the processes of root water uptake during the daytime and soil moisture replenishment during the nighttime (Nachabe et al., 2005). Additionally, the model represents water exchange between roots and the surrounding soil matrix as described by equation (2), which can result in positive (from soil to roots) or negative (from roots to soil) fluxes at different depths. The resulting net vertical water redistribution through roots is referred to as "hydraulic redistribution" (Dawson, 1993; Prieto et al., 2012). However, the effects of hydraulic redistribution are insignificant for the current homogeneous soil profile because the root surface area density in the upper dry layers is too low as a result of root optimization (Schymanski et al., 2008), as shown in Figure 8c. Furthermore, the unsaturated hydraulic conductivity of the dry soil surrounding the roots is also too low to yield significant effects. These results are consistent with the field study of Yuan et al. (2014), which indicated that soil moisture in the shallow layers does not exhibit diurnal variations, thereby suggesting that hydraulic lift is not a controlling process at this site.

5. Discussion and Conclusions

In this paper, we implemented VOM-ROOT, a soil moisture-responsive root dynamics scheme (Schymanski et al., 2008), in Noah-MP through exchanges of the soil moisture conditions and the vertical distribution of root density between the models. The dynamic root model describes the optimization of vertical root distribution in response to changes in subsurface water conditions, which allows plants to maintain a sufficient amount of water to meet the water demand for transpiration.

We applied the coupled Noah-MP/VOM-ROOT model to a riparian *Tamarix* spp. stand in a hyperarid area in northwestern China. We conducted two 1-D experiments: one with a static water table depth of 5.65 m (DYN-CON) and the other with the dynamic water table depth of the observed, varying from 5.0 to 6.5 m (DYN-VAR). The transpiration modeled by DYN-VAR was 472 mm/yr (92.3% of *ET*); the modeled evaporation from the canopy and soil surface was approximately 39.5 mm/yr (7.7% of *ET*), which is close to the observed precipitation (approximately 35 mm/yr). At this dry riparian site, transpiration is primarily supplied by direct root water uptake from the capillary fringe and groundwater that is recharged by lateral groundwater flow, whereas evaporation from the canopy and soil surface is primarily supplied by precipitation. The coupled Noah-MP/VOM-ROOT simulations indicated that up to 84% of the water lost through transpiration was obtained from the saturated zone through direct root water uptake.

The root systems of desert phreatophytes have a remarkable ability to adapt to groundwater dynamics (Naumburg et al., 2005; Orellana et al., 2012), resulting in vertically optimized active roots that respond to water table dynamics. In this study, the root surface area density in both the saturated and the unsaturated zones was optimized through VOM-ROOT, whereas the rooting depth in the saturated zone was calibrated against the observed *ET*. For DYN-VAR, the resulting rooting depth was 5.70 m and the root fraction below 5.0 m averaged over the growing seasons was 0.44. These results are consistent with the observations of Xu et al. (2011), which suggested that roots within the capillary fringe and the underlying saturated zone account for approximately 40% of the total roots. The calibrated rooting depth is almost the same with the average water table depth, suggesting the rooting depth follows the water table dynamics, and the rooting depth can be roughly prescribed as the observed average water table depth in the coupled Noah-MP/VOM-ROOT model.

As noted by Šimůnek and Hopmans (2009), for macroscopic root water uptake models, a priori knowledge of root distribution is extremely important when uncompensated root water uptake schemes are considered. Our results suggest that the VOM-ROOT model (Schymanski et al., 2008) implemented in the Noah-MP is capable of predicting the root distribution needed to simulate water and energy exchanges between phreatophytic vegetation and the atmosphere. Such root optimization models provide a water potential gradient-based approach to describe the compensation mechanisms for the root water uptake (Gou & Miller, 2014; Teodosio et al., 2017). However, the optimization scheme is more explicit than the compensation schemes that use the root adaptability factor, which is difficult to determine for various soil and

vegetation types. Additionally, the optimization scheme is more compatible for future coupling with root biomass predicted by the Noah-MP's plant physiology and carbon allocation schemes.

For deep-rooted vegetation, instead of a standard rooting depth of 2 m in the land surface models, optimized large rooting depths can significantly improve the simulation of root water uptake and the associated latent heat flux (Kleidon & Heimann, 1998; Schymanski et al., 2015). In our simulations, we had to prescribe (or calibrate) the rooting depth in VOM-ROOT as a static parameter, although the root surface area density was predicted using the optimization scheme. We anticipate that together with calibrating the rooting depth, the optimization schemes might also be able to simulate the functional response of phreatophytic roots.

Root dynamics depend on plant physiological characteristics, groundwater dynamics, and soil types, among other variables (Naumburg et al., 2005; Norby & Jackson, 2000). In addition, recent research (e.g., Moffett & Gorelick, 2016) has highlighted the importance of geochemical contributions to self-organized vegetation zonation, including changes in root distribution shape and density under different salinity stresses (Coppola et al., 2015). Therefore, understanding the combined effects of water and salinity stresses on the redistribution of the root system remains a major challenge for simulations of root water uptake processes (Skaggs et al., 2006). Finally, a vertically layered texture has the potential to significantly affect vertical soil water movement and redistribution and should be represented in future models.

In arid riparian regions, the dominant water sources for plant transpiration can rapidly alternate between soil water during the wet season and groundwater during the dry seasons (Gou & Miller, 2014) through root optimization controlled by water availability (Teuling et al., 2006). For groundwater-dependent vegetation, groundwater contributes significantly to the root water uptake, though this contribution may vary widely depending on changes in soil thickness and water table regimes (Lowry & Loheide, 2010). This study represents a step toward a full representation of the interactions between root dynamics and soil water/groundwater dynamics and provides insight into the role of water table dynamics in controlling land-atmosphere interactions (Anyah et al., 2008; Green et al., 2011; Lowry & Loheide, 2010).

Acknowledgments
This research was supported by grants from the National Natural Science Foundation of China (41671023, 41571029, and 41271050) and the NSFC-RFBR Program 2018–2019 (41811130023 and 18-55-53025 ΓΦΕΗ_a). We thank Deliang Chen at the University of Gothenburg for his helpful advice. We also extend special thanks to Stanislaus J. Schymanski at the Swiss Federal Institute of Technology, Zurich, for help and suggestions in coupling VOM-ROOT with Noah-MP. The first author thanks the China Scholarship Council (201304910063) for its support of this work. Guo-Yue Niu is grateful for support from the NASA MAP Program (80NSSC17K0352), the National Science Foundation for Critical Zone Observatory (NSF-EAR-1331408), and the NSF Macrosystem Biology (NSF-EF 1065790). The authors gratefully acknowledge the editor, D. Scott Mackay, the anonymous associate editor, and three reviewers for their valuable comments and suggestions, which have led to substantial improvements over an earlier version of the manuscript. Data used in this study are archived at http://doi.org/10.5281/zenodo.1172512; contact Ping Wang (wangping@igsnrr.ac.cn) for access to the data.

References

Anwar, M., & Yin, L. (1997). Estimation of the above-ground biomass of *Tamarix* spp. (in Chinese). *Environmental Protection of Xinjiang*, *19*(1), 46–50.

Anyah, R. O., Weaver, C. P., Miguez-Macho, G., Fan, Y., & Robock, A. (2008). Incorporating water table dynamics in climate modeling. 3: Simulated groundwater influence on coupled land-atmosphere variability. *Journal of Geophysical Research*, *113*, D07103. https://doi.org/10.1029/2007JD009087

Canham, C., Froend, R., Stock, W., & Davies, M. (2012). Dynamics of phreatophyte root growth relative to a seasonally fluctuating water table in a Mediterranean-type environment. *Oecologia*, *170*(4), 909–916.

Chen, F., & Dudhia, J. (2001). Coupling an advanced land surface-hydrology model with the Penn State-NCAR MM5 modeling system. Part I: Model implementation and sensitivity. *Monthly Weather Review*, *129*(4), 569–585.

Clapp, R. B., & Hornberger, G. M. (1978). Empirical equations for some soil hydraulic properties. *Water Resources Research*, *14*(4), 601–604.

Cleverly, J. R., Dahm, C. N., Thibault, J. R., McDonnell, D. E., & Allred Coonrod, J. E. (2006). Riparian ecohydrology: Regulation of water flux from the ground to the atmosphere in the Middle Rio Grande, New Mexico. *Hydrological Processes*, *20*(15), 3207–3225.

Collatz, G. J., Ball, J. T., Grivet, C., & Berry, J. A. (1991). Physiological and environmental regulation of stomatal conductance, photosynthesis and transpiration: A model that includes a laminar boundary layer. *Agricultural and Forest Meteorology*, *54*(2), 107–136.

Collatz, G., Ribas-Carbo, M., & Berry, J. (1992). Coupled photosynthesis-stomatal conductance model for leaves of C_4 plants. *Functional Plant Biology*, *19*(5), 519–538.

Cooper, D. J., Sanderson, J. S., Stannard, D. I., & Groeneveld, D. P. (2006). Effects of long-term water table drawdown on evapotranspiration and vegetation in an arid region phreatophyte community. *Journal of Hydrology*, *325*(1–4), 21–34.

Coppola, A., Chaali, N., Dragonetti, G., Lamaddalena, N., & Comegna, A. (2015). Root uptake under non-uniform root-zone salinity. *Ecohydrology*, *8*(7), 1363–1379.

Cowan, I. R. (1978). Stomatal behaviour and environment. *Advances in Botanical Research*, *4*, 117–228.

Dawson, T. E. (1993). Hydraulic lift and water use by plants: Implications for water balance, performance and plant-plant interactions. *Oecologia*, *95*(4), 565–574.

Devitt, D. A., Fenstermaker, L. F., Young, M. H., Conrad, B., Baghzouz, M., & Bird, B. M. (2011). Evapotranspiration of mixed shrub communities in phreatophytic zones of the Great Basin region of Nevada (USA). *Ecohydrology*, *4*(6), 807–822.

Dickinson, R. E., Shaikh, M., Bryant, R., & Graumlich, L. (1998). Interactive canopies for a climate model. *Journal of Climate*, *11*(11), 2823–2836.

Eamus, D., Froend, R., Loomes, R., Hose, G., & Murray, B. (2006). A functional methodology for determining the groundwater regime needed to maintain the health of groundwater-dependent vegetation. *Australian Journal of Botany*, *54*(2), 97–114.

Eamus, D., Zolfaghar, S., Villalobos-Vega, R., Cleverly, J., & Huete, A. (2015). Groundwater-dependent ecosystems: Recent insights from satellite and field-based studies. *Hydrology and Earth System Sciences*, *19*(10), 4229–4256.

Ehleringer, J. R., & Dawson, T. E. (1992). Water uptake by plants: Perspectives from stable isotope composition. *Plant, Cell & Environment*, *15*(9), 1073–1082.

Ek, M. B., Mitchell, K. E., Lin, Y., Rogers, E., Grunmann, P., Koren, V., et al. (2003). Implementation of Noah land surface model advances in the National Centers for Environmental Prediction operational mesoscale Eta model. *Journal of Geophysical Research: Atmospheres*, *108*(D22), 8851. https://doi.org/10.1029/2002JD003296

Engel, V., Jobbágy, E. G., Stieglitz, M., Williams, M., & Jackson, R. B. (2005). Hydrological consequences of Eucalyptus afforestation in the Argentine Pampas. *Water Resources Research*, *41*, W10409. https://doi.org/10.1029/2004WR003761

Fan, Y., Miguez-Macho, G., Jobbágy, E. G., Jackson, R. B., & Otero-Casal, C. (2017). Hydrologic regulation of plant rooting depth. *Proceedings of the National Academy of Sciences of the United States of America*, *114*(40), 10572–10577.

Farquhar, G. D., von Caemmerer, S., & Berry, J. A. (1980). A biochemical model of photosynthetic CO_2 assimilation in leaves of C_3 species. *Planta*, *149*(1), 78–90.

Feddes, R. A., Kowalik, P. J., & Zaradny, H. (1978). *Simulation of field water use and crop yield, Simul. Monogr*. (189 p.). Wageningen, the Netherlands: Cent. for Agric. Publ. and Doc.

Fenner, P., Brady, W. W., & Patton, D. R. (1984). Observations on seeds and seedlings of Fremont cottonwood. *Desert Plants*, *6*(1), 55–58.

Foken, T. (2008). The energy balance closure problem: An overview. *Ecological Applications*, *18*(6), 1351–1367.

Gao, Y., Li, K., Chen, F., Jiang, Y., & Lu, C. (2015). Assessing and improving Noah-MP land model simulations for the central Tibetan Plateau. *Journal of Geophysical Research: Atmospheres*, *120*, 9258–9278. https://doi.org/10.1002/2015JD023404

Gary, H. L. (1963). Root distribution of five-stamen *Tamarisk*, *Seepwillow* and *Arrowweed*. *Forest Science*, *9*(3), 311–314.

Gayler, S., Wöhling, T., Grzeschik, M., Ingwersen, J., Wizemann, H.-D., Warrach-Sagi, K., et al. (2014). Incorporating dynamic root growth enhances the performance of Noah-MP at two contrasting winter wheat field sites. *Water Resources Research*, *50*, 1337–1356. https://doi.org/10.1002/2013WR014634

Gim, H.-J., Park, S. K., Kang, M., Thakuri, B. M., Kim, J., & Ho, C.-H. (2017). An improved parameterization of the allocation of assimilated carbon to plant parts in vegetation dynamics for Noah-MP. *Journal of Advances in Modeling Earth Systems*, *9*(4), 1776–1794.

Glenn, E. P., & Nagler, P. L. (2005). Comparative ecophysiology of *Tamarix ramosissima* and native trees in western U.S. riparian zones. *Journal of Arid Environments*, *61*(3), 419–446.

Glenn, E. P., Nagler, P. L., Morino, K., & Hultine, K. (2013). Phreatophytes under stress: Transpiration and stomatal conductance of saltcedar (*Tamarix* spp.) in a high-salinity environment. *Plant and Soil*, *371*(1–2), 655–672.

Gou, S., & Miller, G. (2014). A groundwater-soil-plant-atmosphere continuum approach for modelling water stress, uptake, and hydraulic redistribution in phreatophytic vegetation. *Ecohydrology*, *7*(3), 1029–1041.

Green, T. R., Taniguchi, M., Kooi, H., Gurdak, J. J., Allen, D. M., Hiscock, K. M., et al. (2011). Beneath the surface of global change: Impacts of climate change on groundwater. *Journal of Hydrology*, *405*(3–4), 532–560.

Gribovszki, Z., Szilágyi, J., & Kalicz, P. (2010). Diurnal fluctuations in shallow groundwater levels and streamflow rates and their interpretation—A review. *Journal of Hydrology*, *385*(1–4), 371–383.

Gries, D., Zeng, F., Foetzki, A., Arndt, S. K., Bruelheide, H., Thomas, F. M., et al. (2003). Growth and water relations of *Tamarix ramosissima* and *Populus euphratica* on Taklamakan desert dunes in relation to depth to a permanent water table. *Plant, Cell & Environment*, *26*(5), 725–736.

Guswa, A. J. (2008). The influence of climate on root depth: A carbon cost-benefit analysis. *Water Resources Research*, *44*, W02427. https://doi.org/10.1029/2007WR006384

Guswa, A. J. (2010). Effect of plant uptake strategy on the water-optimal root depth. *Water Resources Research*, *46*, W09601. https://doi.org/10.1029/2010WR009122

Han, S., & Hu, H. (2012). Spatial variations and temporal changes in potential evaporation in the Tarim Basin, northwest China (1960–2006): Influenced by irrigation? *Hydrological Processes*, *26*(20), 3041–3051.

Hao, X., Zhang, R., Zhang, R., & Kravchenko, A. (2005). Effects of root density distribution models on root water uptake and water flow under irrigation. *Soil Science*, *170*(3), 167–174.

Heusinkveld, B. G., Jacobs, A. F. G., Holtslag, A. A. M., & Berkowicz, S. M. (2004). Surface energy balance closure in an arid region: Role of soil heat flux. *Agricultural and Forest Meteorology*, *122*(1–2), 21–37.

Horton, J. L., & Clark, J. L. (2001). Water table decline alters growth and survival of *Salix gooddingii* and *Tamarix chinensis* seedlings. *Forest Ecology and Management*, *140*(2–3), 239–247.

Hultine, K. R., Nagler, P. L., Morino, K., Bush, S. E., Burtch, K. G., Dennison, P. E., et al. (2010). Sap flux-scaled transpiration by tamarisk (*Tamarix* spp.) before, during and after episodic defoliation by the saltcedar leaf beetle (*Diorhabda carinulata*). *Agricultural and Forest Meteorology*, *150*(11), 1467–1475.

Jackson, R. B., Schenk, H. J., Jobbágy, E. G., Canadell, J., Colello, G. D., Dickinson, R. E., et al. (2000). Belowground consequences of vegetation change and their treatment in models. *Ecological Applications*, *10*(2), 470–483.

Jaoudé, R. A., de Dato, G., & De Angelis, P. (2012). Photosynthetic and wood anatomical responses of *Tamarix africana* Poiret to water level reduction after short-term fresh- and saline-water flooding. *Ecological Research*, *27*(5), 857–866.

Jaoudé, R. A., de Dato, G., Palmegiani, M., & De Angelis, P. (2013). Impact of fresh and saline water flooding on leaf gas exchange in two Italian provenances of *Tamarix africana* Poiret. *Plant Biology*, *15*, 109–117.

Jury, W. A., & Horton, R. (2004). *Soil physics* (6th ed.). Hoboken, NJ: John Wiley.

Kleidon, A., & Heimann, M. (1998). A method of determining rooting depth from a terrestrial biosphere model and its impacts on the global water and carbon cycle. *Global Change Biology*, *4*(3), 275–286.

Kranjcec, J., Mahoney, J. M., & Rood, S. B. (1998). The responses of three riparian cottonwood species to water table decline. *Forest Ecology and Management*, *110*(1–3), 77–87.

Kuzminsky, E., De Angelis, P., Abou Jaoudé, R., Abbruzzese, G., Terzoli, S., Angelaccio, C., et al. (2014). Biodiversity of Italian *Tamarix* spp. populations: Their potential as environmental and productive resources. *Rendiconti Lincei. Scienze Fisiche e Naturali*, *25*(4), 439–452.

Lacointe, A. (2000). Carbon allocation among tree organs: A review of basic processes and representation in functional-structural tree models. *Annals of Forest Science*, *57*(5), 521–533.

Le Maitre, D. C., D. Scott, F., & Colvin, C. (1999). A review of information on interactions between vegetation and groundwater. *Water Research Commission*, *25*(2), 137–152.

Loheide, S. P., II, Butler, J. J., Jr., & Gorelick, S. M. (2005). Estimation of groundwater consumption by phreatophytes using diurnal water table fluctuations: A saturated-unsaturated flow assessment. *Water Resources Research*, *41*, W07030. https://doi.org/10.1029/2005WR003942

Lowry, C. S., & Loheide, S. P. II (2010). Groundwater-dependent vegetation: Quantifying the groundwater subsidy. *Water Resources Research*, *46*, W06202. https://doi.org/10.1029/2009WR008874

Ma, N., Niu, G.-Y., Xia, Y., Cai, X., Zhang, Y., Ma, Y., et al. (2017). A systematic evaluation of Noah-MP in simulating land-atmosphere energy, water, and carbon exchanges over the continental United States. *Journal of Geophysical Research: Atmospheres*, *122*, 12245–12268. https://doi.org/10.1002/2017JD027597

Meinzer, O. E. (1927). Plants as indicators of ground water (U.S. Geol. Surv. Water-Supply Paper 577, 95 p.). Washington, DC: U.S. Government Printing Office.
Meyboom, P. (1965). Three observations on streamflow depletion by phreatophytes. *Journal of Hydrology*, *2*(3), 248–261.
Miller, G. R., Chen, X., Rubin, Y., Ma, S., & Baldocchi, D. D. (2010). Groundwater uptake by woody vegetation in a semiarid oak savanna. *Water Resources Research*, *46*, W10503. https://doi.org/10.1029/2009WR008902
Moffett, K. B., & Gorelick, S. M. (2016). Relating salt marsh pore water geochemistry patterns to vegetation zones and hydrologic influences. *Water Resources Research*, *52*, 1729–1745. https://doi.org/10.1002/2015WR017406
Nachabe, M., Shah, N., Ross, M., & Vomacka, J. (2005). Evapotranspiration of two vegetation covers in a shallow water table environment. *Soil Science Society of America Journal*, *69*(2), 492–499.
Nagler, P. L., Glenn, E. P., Didan, K., Osterberg, J., Jordan, F., & Cunningham, J. (2008). Wide-area estimates of stand structure and water use of *Tamarix* spp. on the Lower Colorado River: Implications for restoration and water management projects. *Restoration Ecology*, *16*(1), 136–145.
Nagler, P. L., Glenn, E. P., Lewis Thompson, T., & Huete, A. (2004). Leaf area index and normalized difference vegetation index as predictors of canopy characteristics and light interception by riparian species on the Lower Colorado River. *Agricultural and Forest Meteorology*, *125*(1–2), 1–17.
Naumburg, E., Mata-Gonzalez, R., Hunter, R. G., McLendon, T., & Martin, D. W. (2005). Phreatophytic vegetation and groundwater fluctuations: A review of current research and application of ecosystem response modeling with an emphasis on great basin vegetation. *Environmental Management*, *35*(6), 726–740.
Nippert, J. B., Butler, J. J., Kluitenberg, G. J., Whittemore, D. O., Arnold, D., Spal, S. E., et al. (2010). Patterns of *Tamarix* water use during a record drought. *Oecologia*, *162*(2), 283–292.
Niu, G.-Y., Yang, Z.-L., Dickinson, R. E., & Gulden, L. E. (2005). A simple TOPMODEL-based runoff parameterization (SIMTOP) for use in global climate models. *Journal of Geophysical Research: Atmospheres*, *110*, D21106. https://doi.org/10.1029/2005JD006111
Niu, G.-Y., Yang, Z.-L., Dickinson, R. E., Gulden, L. E., & Su, H. (2007). Development of a simple groundwater model for use in climate models and evaluation with Gravity Recovery and Climate Experiment data. *Journal of Geophysical Research*, *112*, D07103. https://doi.org/10.1029/2006JD007522
Niu, G.-Y., Yang, Z. L., Mitchell, K. E., Chen, F., Ek, M. B., Barlage, M., et al. (2011). The community Noah land surface model with multiparameterization options (Noah-MP): 1. Model description and evaluation with local-scale measurements. *Journal of Geophysical Research*, *116*, D12109. https://doi.org/10.1029/2010JD015139
Norby, R. J., & Jackson, R. B. (2000). Root dynamics and global change: Seeking an ecosystem perspective. *New Phytologist*, *147*(1), 3–12.
Oleson, K. W., Lawrence, D. M., Gordon, B., Flanner, M. G., Kluzek, E., Peter, J., et al. (2010). *Technical description of version 4.0 of the community land model (CLM)* (NCAR Tech. Note NCAR/TN-478+STR, 257 p.). Boulder, CO: National Center for Atmospheric Research.
Orellana, F., Verma, P., Loheide, S. P., II., & Daly, E. (2012). Monitoring and modeling water-vegetation interactions in groundwater-dependent ecosystems. *Reviews of Geophysics*, *50*, RG3003. https://doi.org/10.1029/2011RG000383
Orians, G. H., & Solbrig, O. T. (1977). A cost-income model of leaves and roots with special reference to arid and semiarid areas. *The American Naturalist*, *111*(980), 677–690.
Prieto, I., Armas, C., & Pugnaire, F. I. (2012). Water release through plant roots: New insights into its consequences at the plant and ecosystem level. *New Phytologist*, *193*(4), 830–841.
Rudd, K., Albertson, J. D., & Ferrari, S. (2014). Optimal root profiles in water-limited ecosystems. *Advances in Water Resources*, *71*, 16–22.
Sala, A., Smith, S. D., & Devitt, D. A. (1996). Water use by *Tamarix ramosissima* and associated phreatophytes in a Mojave desert floodplain. *Ecological Applications*, *6*(3), 888–898.
Schaap, M. G., Leij, F. J., & van Genuchten, M. T. (2001). Rosetta: A computer program for estimating soil hydraulic parameters with hierarchical pedotransfer functions. *Journal of Hydrology*, *251*(3–4), 163–176.
Schymanski, S. J. (2007). *Transpiration as the leak in the carbon factory: A model of self-optimising vegetation* (PhD thesis). Crawley, WA: University of Western Australia.
Schymanski, S. J., Roderick, M. L., & Sivapalan, M. (2015). Using an optimality model to understand medium- and long-term responses of vegetation water use to elevated atmospheric CO_2 concentrations. *AoB Plants*, *7*, plv060.
Schymanski, S. J., Sivapalan, M., Roderick, M. L., Beringer, J., & Hutley, L. B. (2008). An optimality-based model of the coupled soil moisture and root dynamics. *Hydrology and Earth System Sciences*, *12*(3), 913–932.
Schymanski, S. J., Sivapalan, M., Roderick, M. L., Hutley, L. B., & Beringer, J. (2009). An optimality-based model of the dynamic feedbacks between natural vegetation and the water balance. *Water Resources Research*, *45*, W01412. https://doi.org/10.1029/2008WR006841
Scott, R. L., Cable, W. L., Huxman, T. E., Nagler, P. L., Hernandez, M., & Goodrich, D. C. (2008). Multiyear riparian evapotranspiration and groundwater use for a semiarid watershed. *Journal of Arid Environments*, *72*(7), 1232–1246.
Scott, R. L., Edwards, E. A., Shuttleworth, W. J., Huxman, T. E., Watts, C., & Goodrich, D. C. (2004). Interannual and seasonal variation in fluxes of water and carbon dioxide from a riparian woodland ecosystem. *Agricultural and Forest Meteorology*, *122*(1–2), 65–84.
Šimůnek, J., & Hopmans, J. W. (2009). Modeling compensated root water and nutrient uptake. *Ecological Modelling*, *220*(4), 505–521.
Skaggs, T. H., van Genuchten, M. T., Shouse, P. J., & Poss, J. A. (2006). Macroscopic approaches to root water uptake as a function of water and salinity stress. *Agricultural Water Management*, *86*(1–2), 140–149.
Smithwick, E. A. H., Lucash, M. S., McCormack, M. L., & Sivandran, G. (2014). Improving the representation of roots in terrestrial models. *Ecological Modelling*, *291*, (0), 193–204.
Sommer, B., & Froend, R. (2011). Resilience of phreatophytic vegetation to groundwater drawdown: Is recovery possible under a drying climate? *Ecohydrology*, *4*(1), 67–82.
Steinwand, A. L., Harrington, R. F., & Or, D. (2006). Water balance for Great Basin phreatophytes derived from eddy covariance, soil water, and water table measurements. *Journal of Hydrology*, *329*(3–4), 595–605.
Stromberg, J. C. (2013). Root patterns and hydrogeomorphic niches of riparian plants in the American Southwest. *Journal of Arid Environments*, *94*, 1–9.
Stromberg, J. C., Beauchamp, V. B., Dixon, M. D., Lite, S. J., & Paradzick, C. (2007). Importance of low-flow and high-flow characteristics to restoration of riparian vegetation along rivers in arid south-western United States. *Freshwater Biology*, *52*(4), 651–679.
Teodosio, B., Pauwels, V. R. N., Loheide, S. P., & Daly, E. (2017). Relationship between root water uptake and soil respiration: A modeling perspective. *Journal of Geophysical Research: Biogeosciences*, *122*, 1954–1968. https://doi.org/10.1002/2017JG003831
Teuling, A. J., Uijlenhoet, R., Hupet, F., & Troch, P. A. (2006). Impact of plant water uptake strategy on soil moisture and evapotranspiration dynamics during drydown. *Geophysical Research Letters*, *33*, L03401. https://doi.org/10.1029/2005GL025019
Tian, Y., Dickinson, R. E., Zhou, L., Zeng, X., Dai, Y., Myneni, R. B., et al. (2004). Comparison of seasonal and spatial variations of leaf area index and fraction of absorbed photosynthetically active radiation from Moderate Resolution Imaging Spectroradiometer (MODIS) and Common Land Model. *Journal of Geophysical Research*, *109*, D01103. https://doi.org/10.1029/2003JD003777

Tron, S., Perona, P., Gorla, L., Schwarz, M., Laio, F., & Ridolfi, L. (2015). The signature of randomness in riparian plant root distributions. *Geophysical Research Letters*, *42*, 7098–7106. https://doi.org/10.1002/2015GL064857

Twine, T. E., Kustas, W. P., Norman, J. M., Cook, D. R., Houser, P. R., Meyers, T. P., et al. (2000). Correcting eddy-covariance flux underestimates over a grassland. *Agricultural and Forest Meteorology*, *103*(3), 279–300.

Vogel, T., Votrubova, J., Dusek, J., & Dohnal, M. (2016). Mesoscopic aspects of root water uptake modeling—Hydraulic resistances and root geometry interpretations in plant transpiration analysis. *Advances in Water Resources*, *88*, 86–96.

Vonlanthen, B., Zhang, X., & Bruelheide, H. (2010). On the run for water—Root growth of two phreatophytes in the Taklamakan Desert. *Journal of Arid Environments*, *74*(12), 1604–1615.

Wang, P., & Pozdniakov, S. P. (2014). A statistical approach to estimating evapotranspiration from diurnal groundwater level fluctuations. *Water Resources Research*, *50*, 2276–2292. https://doi.org/10.1002/2013WR014251

Wang, P., Grinevsky, S. O., Pozdniakov, S., Yu, P. J., Dautova, D., Min, S., et al. (2014b). Application of the water table fluctuation method for estimating evapotranspiration at two phreatophyte-dominated sites under hyper-arid environments. *Journal of Hydrology*, *519*(Part B), 2289–2300.

Wang, P., Yu, J., Pozdniakov, S. P., Grinevsky, S. O., & Liu, C. (2014a). Shallow groundwater dynamics and its driving forces in extremely arid areas: A case study of the lower Heihe River in northwestern China. *Hydrological Processes*, *28*(3), 1539–1553.

Wang, P., Zhao, C.-Y., & Li, J. (2012). Effects of groundwater depth and mineralization degree on photosynthesis and growth of *Tamarix Ramosissima* seedlings (in Chinese with English abstract). *Bulletin of Soil and Water Conservation*, *32*(2), 84–89.

Warren, J. M., Hanson, P. J., Iversen, C. M., Kumar, J., Walker, A. P., & Wullschleger, S. D. (2015). Root structural and functional dynamics in terrestrial biosphere models—Evaluation and recommendations. *New Phytologist*, *205*(1), 59–78.

Westoby, M. (1979). Elements of a theory of vegetation dynamics in arid rangelands. *Israel Journal of Botany*, *28*(3–4), 169–194.

White, W. N. (1932). *A method of estimating ground-water supplies based on discharge by plants and evaporation from soil: Results of investigation in Escalante Valley, Utah* (U.S. Geol. Surv. Water Supply Paper 659-A, 105 p.). Washington, DC: U.S. Government Printing Office.

Wilson, K., Goldstein, A., Falge, E., Aubinet, M., Baldocchi, D., Berbigier, P., et al. (2002). Energy balance closure at FLUXNET sites. *Agricultural and Forest Meteorology*, *113*(1–4), 223–243.

Xu, G.-Q., Li, Y., & Xu, H. (2011). Seasonal variation in plant hydraulic traits of two co-occurring desert shrubs, *Tamarix ramosissima* and *Haloxylon ammodendron*, with different rooting patterns. *Ecological Research*, *26*(6), 1071–1080.

Ye, Z. X., Chen, Y. N., Li, W. H., Yan, Y., & Wan, J. H. (2009). Groundwater fluctuations induced by ecological water conveyance in the lower Tarim River, Xinjiang, China. *Journal of Arid Environments*, *73*(8), 726–732.

Yuan, G., Zhang, P., Shao, M-A., Luo, Y., & Zhu, X. (2014). Energy and water exchanges over a riparian *Tamarix* spp. stand in the lower Tarim River basin under a hyper-arid climate. *Agricultural and Forest Meteorology*, *194*, 144–154.

Zeng, F., Zhang, X., & Li, X. (2002). A review on the water physiological characteristics of *Tamarix* and its prospect (in Chinese with English abstract). *Chinese Journal of Applied Ecology*, *13*(5), 611–614.

Zhang, P. (2015). *Research on the impact of groundwater decline on the evapotranspiration of Tamarix stand in the lower reaches of Tarim River* (in Chinese with English abstract) (PhD thesis, 120 p.). Beijing, China: University of Chinese Academy of Sciences.